PLOS ONE

RESEARCH ARTICLE

A computational model of stem cell molecular mechanism to maintain tissue homeostasis

Najme Khorasani[1◉], Mehdi Sadeghi[2,3◉], Abbas Nowzari-Dalini[1◉]*

1 School of Mathematics, Statistics and Computer Science, College of Science, University of Tehran, Tehran, Iran, 2 National Institute of Genetic Engineering and Biotechnology (NIGEB), Tehran, Iran, 3 School of Biological Sciences, Institute for Research in Fundamental Sciences (IPM), Tehran, Iran

◉ These authors contributed equally to this work.
* nowzari@ut.ac.ir

Abstract

Stem cells, with their capacity to self-renew and to differentiate to more specialized cell types, play a key role to maintain homeostasis in adult tissues. To investigate how, in the dynamic stochastic environment of a tissue, non-genetic diversity and the precise balance between proliferation and differentiation are achieved, it is necessary to understand the molecular mechanisms of the stem cells in decision making process. By focusing on the impact of stochasticity, we proposed a computational model describing the regulatory circuitry as a tri-stable dynamical system to reveal the mechanism which orchestrate this balance. Our model explains how the distribution of noise in genes, linked to the cell regulatory networks, affects cell decision-making to maintain homeostatic state. The noise effect on tissue homeostasis is achieved by regulating the probability of differentiation and self-renewal through symmetric and/or asymmetric cell divisions. Our model reveals, when mutations due to the replication of DNA in stem cell division, are inevitable, how mutations contribute to either aging gradually or the development of cancer in a short period of time. Furthermore, our model sheds some light on the impact of more complex regulatory networks on the system robustness against perturbations.

Introduction

Throughout development, stem cells play a key role during multiple morphogenetic processes, such as tissue growth, regeneration, and repair. Stem cells are characterized by their capacity to self-renew and to differentiate to more specialized cell types [1, 2] and a balance between these two processes is necessary to maintain homeostasis in adult tissues [3–6]. Abnormalities in the differentiation or imbalance between proliferation rate and tissue demand can lead to dysfunctional tissues or tumorigenesis. On the other hand, to develop a tissue with hundreds of different cell types from a single stem cell, a non-genetic diversifying mechanism is required. Hence, understanding the underlying mechanisms which regulate the non-genetic diversity and orchestrate the stem cell proliferation/differentiation balance in the dynamic stochastic environment of a tissue is a central challenge in adult stem cell biology [7].

Stochasticity is an inevitable part of most cellular processes (including cell division) and arises from a plenitude of sources such as variation in gene expression, metabolic activities, protein and RNA degradation, etc [8–10, 11]. This stochsticity, also called intrinsic noise, which results from the probabilistic nature of any biochemical system with a low number of reacting molecules, can lead to cell-to-cell variability during development [11]. Despite the presence of noise, a precise and robust regulation of key reactions in the cell is required for survival and functionality. An increasing number of theoretical and experimental studies are aimed at unraveling the importance of noise in such robust biological processes [11–13]. It is known that biological systems can utilize and regulate this stochasticity to improve their fitness via phenotypic variations [14, 15] and population heterogeneity [10, 16, 17, 11]. During division process, a stem cell utilizes a stochastic cell-fate decision making process, to divide either symmetrically to two differentiated (DD-division) or two new stem cells (SS-division), or asymmetrically to one differentiated and one stem cell (SD-division) [18, 19]. In an adult tissue, in homeostasis state, a perturbation leading to a dominant rate of any of the symmetric division types causes imbalance between proliferation and differentiation, which consequently diminishes the phenotypic diversity. Therefore, a robustly regulated stochastic decision-making process enhances morphogenetic processes by maintaining both proliferation/differentiation balance to avoid tissue depletion or abnormal growth [2, 5, 6] and a non-genetic diversity which is critical to the survival of living systems in noisy environments [20–25]. Cellular regulatory networks are known to play a crucial role in adjusting the decision-making mechanism by considering the effects from permanent intrinsic noise associated with living cells. Such regulatory networks have been studied extensively in a variety of organisms spanning from viruses to mammals [20]. These networks are known to control decision making from viruses [26–28] to bacteria [29–32], yeast [33] and human embryonic stem cells [34–38].s

Taking into account the noisy dynamics of a small number of contributing determinants associated with intracellular processes, it is necessary to utilize a stochastic model to gain a better understanding of the behaviour of such regulatory networks. In this model, the system state is described as quantized fractions of full capacity of each determinant and can evolve stochastically over time [39]. Therefore, the probability of the system being in a given state changes with time, and cell character cannot be predicted deterministically as it is influenced by the intrinsic noise [39, 11]. To simulate the time evolution, it is suitable to use Gillespie algorithm which is proven effective for describing the trajectory of systems including a small number of determinants driven by inherent fluctuations [40, 11]. Averaging over enough simulation runs can provide us with an asymptotic approximation to the exact numerical solution of the master equation without having to deal with intractable mathematical solutions.

By focusing on the impact of stochasticity during cell-fate decision-making process, here, we propose a computational model to reveal the mechanism which regulates the proliferation/differentiation balance in a hypothetical adult tissue. In the most simple model, it is assumed that a developing tissue, consisting of stem cells and two differentiated cell types, has the tendency to maintain a homeostatic state. The proposed model is defined based on five material principles which has been discussed in [10] to study biofilm formation and they are reconsidered as follows i) stochasticity due to an intrinsic noise is a fundamental part of any living cell [10, 17, 41–46]. ii) the non-deterministic position of the cell division plane and nonuniform distribution of determinants in the cell imply that the cytoplasmic molecules are distributed randomly among daughter cells during cell division [10, 47–53]. iii) determination of cell fate by an internal switch upon the completion of cell division [20, 54]. Cell fate is assumed fixed during cell life cycle [10]. iv) the decision bias in the internal switch is determined by model parameters representing interactions between the switch elements [10]. v) a switch with more contributing components would be more stable against environmental fluctuations [10, 36]. In

terms of Waddington landscape, it means that more complex switches lead to deeper valleys from where cells could not easily leave in the presence of stochastic fluctuations.

Inspired by previous studies that revealed the impact of regulatory networks on the stability of biological systems [14, 27, 33, 41, 55–58, 11], here, we introduce a tristable switch described by a set of ordinary differential equations (ODEs) which is a formal framework to study the regulatory circuitries [36, 59, 60–63]. The three stable steady states of the system represent one stem cell, and two bifurcated lineages as two distinct cell types differentiated from a common ancestor. The evolution of our inherently stochastic system is simulated by the Gillespie algorithm.

The overall outcome of our model implies that the presence of controlled noise in a population of genetically similar cells with the same environmental condition is necessary to develop population heterogeneity and also homeostasis. Furthermore, by changing the parameters in cell regulatory switches, we investigate cellular decision-making bias emanating from the stochastic environmental factors. We show that, by having enough information about the noise, predicting the cell fate after cell division is possible and that, the offspring inherit these information. Finally, to further illustrate how a transition from homeostasis to tissue depletion or abnormal growth occur in our model, we explore the behaviour of the populations consisting of cells with mutated internal switches. We show that the switches with more contributing elements are more robust against mutations. Although mutations in the stem cell usually triggers differentiation and consequently rapid depletion of stem cell population over time, accumulation of mutations leads to rapid proliferation of stem cells which is a potential indication of cancer initiation.

Materials and methods

Cell growth and division in the population

To study the regulatory mechanism which provides the proliferation/differentiation balance in homeostatic state, we proposed a computational model described by a set of ordinary differential equations (ODEs) which was previously used in several studies to model the regulatory circuitries as tri-stable dynamical systems [36, 59]. The following set of ODEs are employed to describe a two-element regulatory switch in our model:

$$
\begin{cases}
\dfrac{dx_1}{dt} = \alpha_{A_{X_1}} \dfrac{x_1^n}{\beta^n + x_1^n} + \alpha_{I_{X_1}} \dfrac{\beta^n}{\beta^n + y_1^n} - \gamma x_1 \\[3ex]
\dfrac{dy_1}{dt} = \alpha_{A_{Y_1}} \dfrac{y_1^n}{\beta^n + y_1^n} + \alpha_{I_{Y_1}} \dfrac{\beta^n}{\beta^n + x_1^n} - \gamma y_1
\end{cases}
\tag{1}
$$

In this model, It is assumed that the cell type is controlled by the relative amount of two cytoplasmic cell fate determinants, namely X_1 and Y_1 whose interactions can be described in a form of a tri-stable regulatory switch (see Fig 1A). The dynamical behavior of the determinants X_1 and Y_1 is studied by considering their mutual repression and self-activation effects which are modeled in the form of a Hill function [10, 27], and their degradation rate. Here, n is the Hill coefficient, β is the effective rate of determinnats synthesis, $\alpha_{A_{X_1}}$ and $\alpha_{A_{Y_1}}$ are self-activation rates, $\alpha_{I_{X_1}}$ and $\alpha_{I_{Y_1}}$ are inhibition rates, and gamma is the degradation rate.

Fig 2A illustrates the described system dynamics which is visualized in the representation of the vector field along the nullclines. The grid point dimensions represent the number of determinants X_1 and Y_1 and each arrow represents the derivative of the determinants showing the most probable direction which the number of determinants tends to be updated to, in each
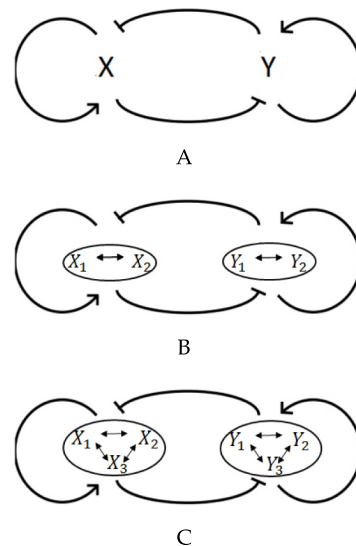
Fig 1. Tri-stable regulatory networks. (A) Two-element switch. (B) Four-element switch. (C) Six-element switch.

time step and based on Eq 1. The red (black) curve represents the x− (y-) nullcline, which are the set of points in phase plane where $\frac{dX1}{dt} = 0$ ($\frac{dY1}{dt} = 0$). The circles represent five fixed points occuring where the nullclines intersect. The direction of the vector field along the nullclines indicate that the white filled circles are unstabe, while the black filled ones are stable representing three attractors of the system.

Fig 2B shows the Waddington's epigenetic landscape which was first described in [64]. It is derived from Eq 1, using the algorithm which is poroposed in [65]. It governs the dynamic behavior of the regulatory switch of our model. The Waddington's landscape portrays branching ridges and valleys which represent the either-or situations which a dividing cell deal with. The cell decisions lead to one of the attractors of the regulatory switch which determines the cell final fate. When a daughter cell is born, it can be represented by a point on the surface, as the quantitative view of the cell, of Fig 2B. The coordinates of the point demonstrate the value of determinants X_1 and Y_1 in the new born cell and determines which path should be followed to reach the final fate (one of the three attractors).

The parameters of Eq 1 are set in such a way that there would be three stable steady states, as it is shown in Fig 2A, corresponding to three different cell fates, stem cell type C (middle attractor) and differentiated cell types A (bottom right attarctor) and B (top left attarctor). The number of determinants of X_1 (Y_1) involved in attractor A (B) is much larger than those of Y_1 (X_1). In attractor C, however, both determinants X_1 and Y_1 are involved in balance. Fig 2C represents the domains of the three attractors, A, B, and C, with three different colors, green, orange, and yellow, respectively. Each daughter cell with specific value of X_1 and Y_1, right after birth, can be shown as a point in Fig 2C. The value of X_1 and Y_1 determines which attractor the cell would be absorbed to, and based on that it defines the domains of three attractors. In other word, each cell fate can be determined and fixed exactly after division based on the number of determinants X_1 and Y_1 in the daughter cell.

The determinant fluctuations are captured by the Gillespie algorithm [10, 40] which is known as the gold standard for simulating models whose stochasticty arises from the small discrete number of reactant molecules [66]. In each time step, two main processes can occur, cell division and the cell determinants interactions. Therefore, five different reactions can
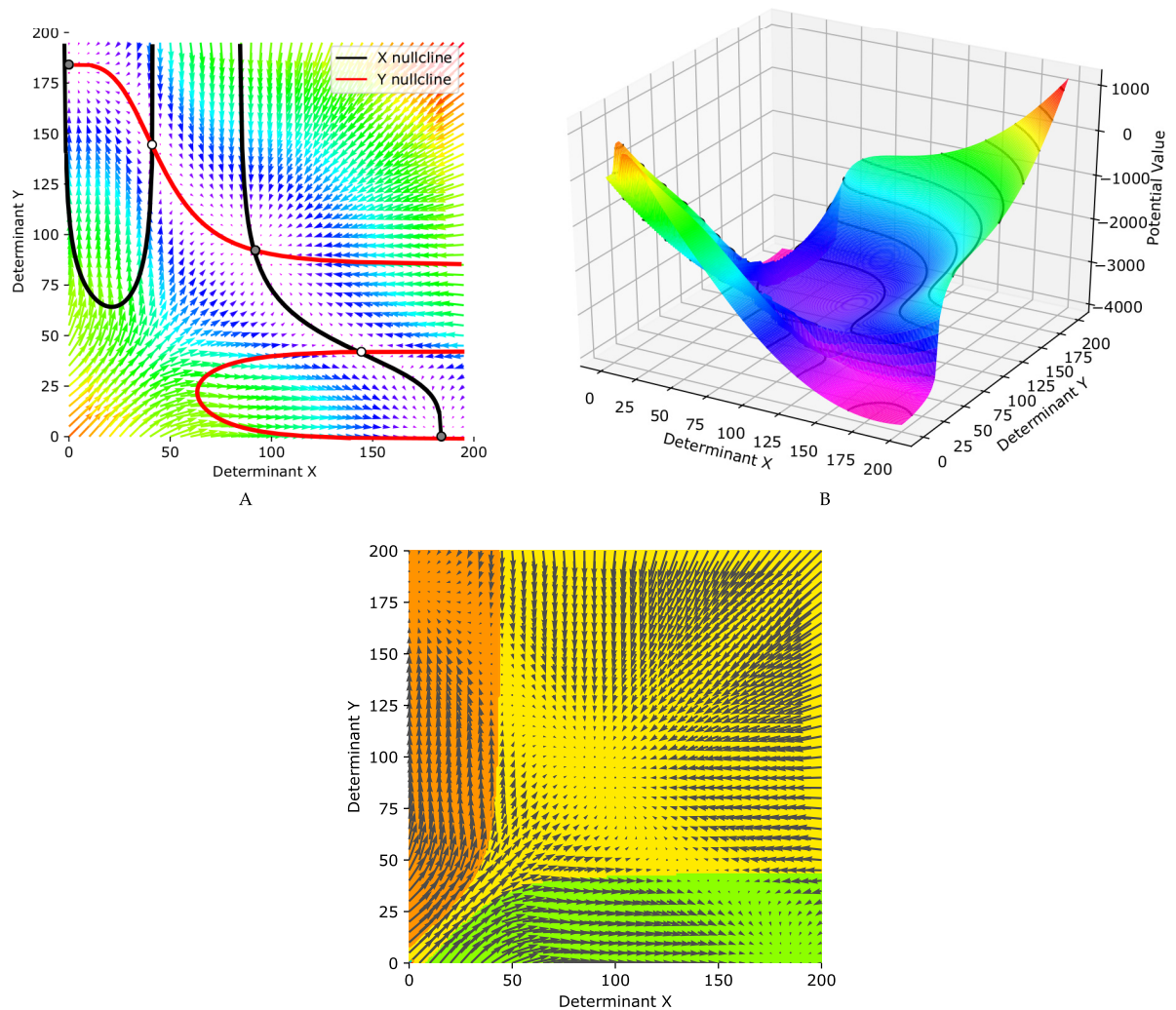
Fig 2. The behaviour of the tri-stable dynamical system. The system represents a regulatory switch consisting of two cell fate determinants, namely *X* and *Y*, with self-activation and mutual-repression interactions. (A) Force-field representation of the tri-stable dynamical system, as well as *X* and *Y* nullclines drawn in red and black. (B) Potential landscape representation of the tri-stable dynamical system. (C) Three attractors domains corresponding to the initial values of determinants in a daughter cell.

potentially happen in each step, division and increasing/decresing of X_1 value, increasing/ decreasing of Y_1 value. In each iteration, one of the above-mentioned processes occurs, time is updated. The simulation continues for a whole cell cycle time *T*, where $T = log(N) * 1.1$ and $N = 184$ ($N = 368$, or $N = 554$), the maximum number of cell determinants in the steady state corresponding to two-element switch (four-, or six-element switch). Hence, one can be sure that each cell can reach an attarctor in this period and it can not easily get out of that [67].

In our model, four reactions, production/degradation of determinant X_1, and production/ degradation of determinant Y_1 has been studied for each cell. In the deterministic manner, the ODE in Eq 1 provides the exact description of these four reactions in our tristable system. The propensity function of the division process would be equal to $1/T$ (Eq 2). In addition, as it is shown in Eqs 3, 4, 5 and 6, four propensity functions are defined corresponding to above-mentioned reactions, respectively. It is worth noting that, Eqs 3, 4, 5 and 6 representing high order reactions could be used only as an approximation with Gillespie algorithm [68]. The

probability of an occurrence of each reaction is proportional to the corresponding propensity function [39, 11, 69].

$$w_1 = 1/T, \tag{2}$$

$$w_2 = \alpha_{A_{X_1}} \frac{x_1^n}{\beta^n + x_1} + \alpha_{I_{X_1}} \frac{\beta^n}{\beta^n + y_1^n}, \tag{3}$$

$$w_3 = \gamma x_1, \tag{4}$$

$$w_4 = \alpha_{A_{Y_1}} \frac{y_1^n}{\beta^n + y_1^n} + \alpha_{I_{Y_1}} \frac{\beta^n}{\beta^n + x_1^n}, \tag{5}$$

$$w_5 = \gamma y_1. \tag{6}$$

At each time step, the Gillespie algorithm determines which reaction occurs. The simulation starts with a population of 50 stem cells, and the number of determinants X_1 and Y_1 are initialized randomly from the middle attractor region (Fig 2A). As the number of determinants in the cell are updating, their corresponding trajectory in the phase plane is changing and finally reaches the domain of their attractor. As mentioned before, for each cell four reactions and one division can potentially happen. As a result, at each time step, $4 \times \sharp cells = 4 \times 50 = 200$ updating reactions and $1 \times \sharp cells = 1 \times 50 = 50$ division processes can potentially occur. Let us define w_i as the propensity function of reaction i, where $i \in \{1, 2, \ldots, 250\}$ (the first 200 indices corresponding to updating reactions, and the rest corresponding to division processes). The probability of occurrence of reaction r is

$$P_r = \frac{w_r}{S_R}, \tag{7}$$

where $R = 250$, and

$$S_r = \sum_{k=1}^{r} w_k, \tag{8}$$

and the reaction r will take place if

$$\frac{S_{r-1}}{S_R} < u_1 < \frac{S_r}{S_R}. \tag{9}$$

The time to the next reaction, Δt, is computed as

$$\Delta t = \frac{1}{\sum_{i=1}^{R} w_i} \ln \frac{1}{u_2} = \frac{1}{S_R} \ln \frac{1}{u_2}, \tag{10}$$

where, u_1, and u_2 are two random numbers between 0 and 1 from a uniform distribution ($\sim U(0, 1)$).

Due to the random distribution of mother cell cytoplasmic molecules between daughter cells as well as the non-deterministic position of the division plane [10, 47–53], we assumed that the distribution of determinants in each daughter cell is binomial [70] with parameters specified according to the whole number of determinants in the mother cell, and probability of success for each trial, $p = \frac{1}{2}$ ($\sim B\left(\sharp X_1, \frac{1}{2}\right)$, or $\sim B\left(\sharp Y_1, \frac{1}{2}\right)$ respectively). At the time of birth,
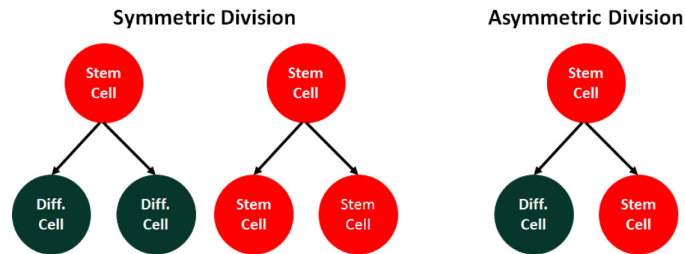
Fig 3. Two different types of divisions, known as symmetric and asymmetric.

each offspring phenotype is determined based on the number of determinants, which is corresponding to a coordinate in the three-region phase plane which is demonstrated in Fig 2C.

Based on the off-springs fate right after division, there are two types of cell division, symmetric and asymmetric (Fig 3). The symmetric division leads to the birth of two stem cells (SS division) or two differentiated cells (DD division), while the asymmetric division generates one stem cell and one differentiated cell (SD division) [19]. In other word, stochastic partitioning of cytoplasm during cell division and the random distribution of molecules in the cytoplasm determines the division types which play a key role in maintaining the proliferation/differentiation balance in homeostatic state.

The aim of this project is understanding the stem cell mechanism in maintaining the proliferation/differentiation balance. Besides, we assume that A, and B cell types are fully differentiated cells which do not proliferate in the tissue. They are replenished by stem cells, perform some functions, and finally are removed from the population by death. It is assumed that they could not influence the stem cells' mechanism. Therefore, here, we have not studied differentiated cells in details. We only observe them as the stem cells' offsprings upon the completion of the cell division and remove them from the simulations without following their fate after that. In other words, in our model, differentiated cells die exactly after their birth. It is worth mentioning here, for the sake of simplicity, we have not studied the apoptosis of stem cells directly. They can be eliminated from the population through differentiation process.

More complex switches

It is assumed that the interactions between two determinants X_1 and Y_1 determine the cell fate right after cell division. The dynamics of the system is described as it is presented in Eq 1. This type of regulatory switches (Fig 1A) are so sensitive to mutations and perturbations that directly affect the cell fate in the population. It suggests designing more complex regulatory networks consisting of a pair of clusters, with multiple elements in each, to determine the final cell fate [36]. These hypothesized clusters have been found in biological regulatory circuitries such as the extended regulatory circuitry of genes associated with PE and EPI cell types (PE markers Gata4, Gata6, Sox17, and Sox7 in one cluster, and EPI markers Nanog, Sox2, and Oct4 in the other cluster) and also TE and ICM cell types (GATA3, CDX2 and EMOES in one cluster and NANOG, SOX2, SALL4, and POU5F1 in the other cluster) during early development in mouse blastocysts [36, 71–84].

The extended switch results in more robustness against perturbations. The buffering effect is achieved by presence of more elements and the positive feed-backs in each cluster [36]. It is expected that this effect would be even stronger in more complex switches, which is in agreement with the Waddington's idea of "*canalisation*" in [85]: "*canalisations are more likely to appear when there are many cross links between the various processes, that is to say when the rate of change of any one variable is affected by the concentrations of many of the other variables*".

In our proposed model, each element in a cluster can have a master or supportive role in cell fate decision making. This model is in contrast with the computational model studied in [36], where all elements of the same group have identical effects in determining cell final fate. In our extended regulatory switch (Fig 1B and 1C), it is supposed that there is a master cell fate indicator in each cluster, and that all other elements support and regulate its effects. In other words, the different elements of the same cluster have different effects on final cell fate, which is supported by experimental observations [38]. It is worth mentioning that, as we are dealing with a symmetric extended regulatory switch, without loss of generality, all of the pairs (X,Y), where X and Y belong to different clusters, could be a potential candidate for master indicators. In spite of identical role of all the elements in the same cluster, it could be assumed that elements of X_1 and Y_1 are the ones which determine the final fate of the daughter cells.

To check the robustness of the extended model, two other ODE systems are designed in Eqs 11 and 12. In Eq 11 (Eq 12) it is assumed that there are two clusters involving in cell fate decision making where they interact with each other in a four-element switch (six-element switch). Besides, clearly the elements in the extended switches can be divided in two groups (x−group and y−group). Determinants in the same group activate each other while they have a negative mutual interaction with the opposite group components.

$$
\begin{cases}
\dfrac{dx_1}{dt} = \alpha_{A_{X_1}} \dfrac{x_1^n + x_2^n}{\beta^n + x_1^n + x_2^n} + \alpha_{I_{X_1}} \dfrac{\beta^n}{\beta^n + y_1^n + y_2^n} - \gamma x_1 \\[3mm]
\dfrac{dx_2}{dt} = \alpha_{A_{X_2}} \dfrac{x_1^n + x_2^n}{\beta^n + x_1^n + x_2^n} + \alpha_{I_{X_2}} \dfrac{\beta^n}{\beta^n + y_1^n + y_2^n} - \gamma x_2 \\[3mm]
\dfrac{dy_1}{dt} = \alpha_{A_{Y_1}} \dfrac{y_1^n + y_2^n}{\beta^n + y_1^n + y_2^n} + \alpha_{I_{Y_1}} \dfrac{\beta^n}{\beta^n + x_1^n + x_2^n} - \gamma y_1 \\[3mm]
\dfrac{dy_2}{dt} = \alpha_{A_{Y_2}} \dfrac{y_1^n + y_2^n}{\beta^n + y_1^n + y_2^n} + \alpha_{I_{Y_2}} \dfrac{\beta^n}{\beta^n + x_1^n + x_2^n} - \gamma y_2
\end{cases}
\tag{11}
$$

$$
\begin{cases}
\dfrac{dx_1}{dt} = \alpha_{A_{X_1}} \dfrac{x_1^n + x_2^n + x_3^n}{\beta^n + x_1^n + x_2^n + x_3^n} + \alpha_{I_{X_1}} \dfrac{\beta^n}{\beta^n + y_1^n + y_2^n + y_3^n} - \gamma x_1 \\[3mm]
\dfrac{dx_2}{dt} = \alpha_{A_{X_2}} \dfrac{x_1^n + x_2^n + x_3^n}{\beta^n + x_1^n + x_2^n + x_3^n} + \alpha_{I_{X_2}} \dfrac{\beta^n}{\beta^n + y_1^n + y_2^n + y_3^n} - \gamma x_2 \\[3mm]
\dfrac{dx_3}{dt} = \alpha_{A_{X_3}} \dfrac{x_1^n + x_2^n + x_3^n}{\beta^n + x_1^n + x_2^n + x_3^n} + \alpha_{I_{X_3}} \dfrac{\beta^n}{\beta^n + y_1^n + y_2^n + y_3^n} - \gamma x_3 \\[3mm]
\dfrac{dy_1}{dt} = \alpha_{A_{Y_1}} \dfrac{y_1^n + y_2^n + y_3^n}{\beta^n + y_1^n + y_2^n + y_3^n} + \alpha_{I_{Y_1}} \dfrac{\beta^n}{\beta^n + x_1^n + x_2^n + x_3^n} - \gamma y_1 \\[3mm]
\dfrac{dy_2}{dt} = \alpha_{A_{Y_2}} \dfrac{y_1^n + y_2^n + y_3^n}{\beta^n + y_1^n + y_2^n + y_3^n} + \alpha_{I_{Y_2}} \dfrac{\beta^n}{\beta^n + x_1^n + x_2^n + x_3^n} - \gamma y_2 \\[3mm]
\dfrac{dy_3}{dt} = \alpha_{A_{Y_3}} \dfrac{y_1^n + y_2^n + y_3^n}{\beta^n + y_1^n + y_2^n + y_3^n} + \alpha_{I_{Y_3}} \dfrac{\beta^n}{\beta^n + x_1^n + x_2^n + x_3^n} - \gamma y_3
\end{cases}
\tag{12}
$$

The four- and six-element switches resemble the former switch in representing a tri-stable system. The number of all elements in the x−group (y−group) involved in attractor A (B) is

much larger than those in the y–group (x–group). In attractor C, all the elements of both groups are involved in balance. However, without loss of generality, we assume that the elements of X_1 and Y_1 are the master indicators which determine the daughter cell fate after division. As it was mentioned before, all other elements in the same cluster (of the switch) only play a key role in buffering the perturbation effects on master determinants. As it is impossible to represent four/six-dimensional plots, the corresponding phase planes of four/six-element switches are plotted in two-dimensional plane. Therefore, both phase planes resemble the one of the two-element switch in Fig 2A, presenting only x_1 and y_1 on x and y axis, respectively.

Results

The homeostatic state in our model

In the homeostatic state, a balance between two processes of differentiation and proliferation is necessary to maintain a fixed number of stem cells in an adult tissue [4, 5]. In our model the parameters in Eqs 1, 11 and 12 are set to the values provided in Table 1. A tri-stable system is obtained with this set of parameters, where, in average, the rate of symmetric division of type DD is equal to that of the SS type, meaning that, in each division, the probability of generating a daughter stem cell is $\simeq 0.50$. In other words, the parameters in Table 1 determine a distribution of determinants, around the middle attractor, which guarantees the proliferation/differentiation balance. By this defined distribution, after each cell division, half of the daughter cells remain in yellow region of Fig 2C (as stem cells), while the other half are born in the green or orange regions of Fig 2C (as differentiated cells). As a result, the number of stem cells in the tissue remains fixed to contribute in future self-renewal and replacement of dead or damaged non-dividing differentiated cells [86].

The parameters of our ODE model (Eq 1) are set through a grid search. It is assumed that $\alpha_{A_{X_1}} = \alpha_{I_{X_1}} = \alpha_{A_{Y_1}} = \alpha_{I_{Y_1}}$. The simulation starts with 1000 populations, each containing of 50 cells, at $t = t_0$, each cell with a two-element regulatory switch, and stops at $t = T$. To compute the time evolution of the cell populations through stochastic simulations, we used the Gillespie algorithm [40]. The stem cell birth (SCB) rate, the probability of generating stem cells in each cell division, is computed at the end of the simulation and represented in Table 1, the first row, the last column. As seen, with this parameter setting, one-half of the daughter cells remain as stem cells and the other half differentiates and maintains the proliferation/differentiation balance. The simulation is repeated on other populations of cells with four- and six-element internal switches (Eqs 11 and 12) and the corresponding parameters are represented in Table 1, the second and third row, respectively.

The perturbation effect in the model

Although a two-element switches could account for describing the interactions between determinants in a cell, it is too sensitive to perturbations which arise from genetic mutations. To be specific, a perturbation in a cell internal switch affects the number of determinants in the cell that could influence the bias of the daughter cells fate toward cell proliferation or differentiation.

Table 1. The parameters set of the model in Homeostasis.

	$\alpha_{A_{X/Y}}$	$\alpha_{I_{X/Y}}$	β	γ	n	SCB
two-element switch	35	35	45	0.38	4	0.5
four-element switch	35	35	47.3	0.38	4	0.5
six-element switch	35	35	48.5	0.38	4	0.5
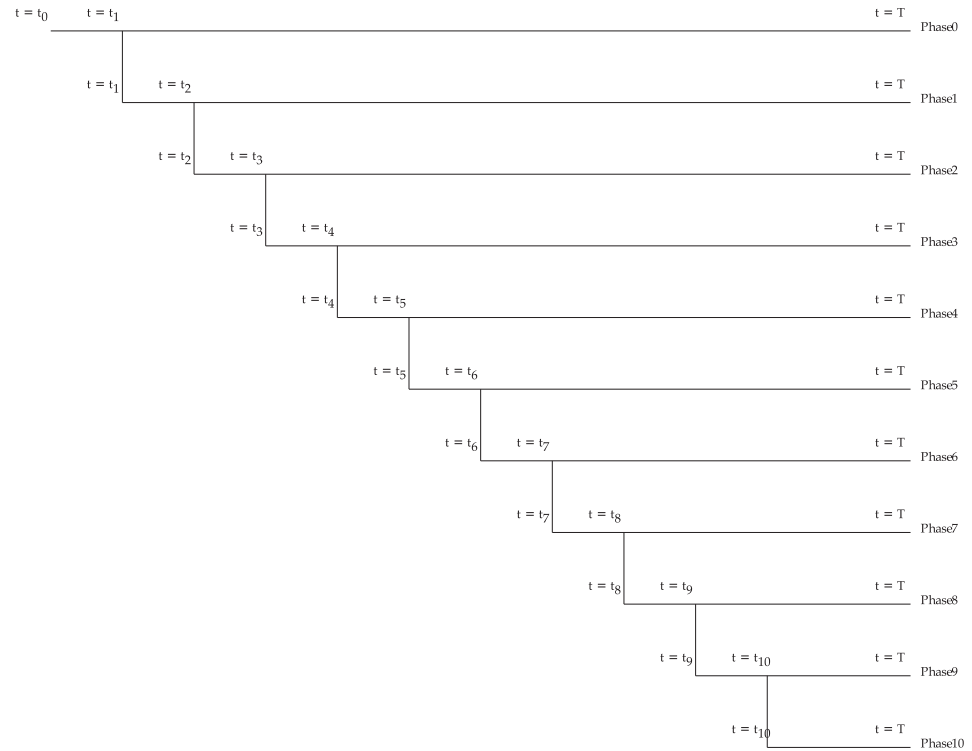
Fig 4. An eleven-phase simulation to study the effect of mutations in the model. Phase 0 starts at $t = t_0$ with 1000 populations, each population containing of 50 cells. In phase k ($k = 1, 3, \ldots, 9$) the state of the system in $t = t_{k+1}$, when all of the cells have gone through at least $k * 2$ divisions, is stored. Phase $k + 1$ starts at $t = t_{k+1}$, the time point at which the kth mutation with the probability value of p occurs to the parameters of the cells' internal switches. All phases finish at $t = T$.

As a result, it affects the the functionality of tissues and organs in replacing damaged or dead cells. A mutation in the system may follows an imbalance in SS and DD division rates which can lead to two different scenarios. First, if the SS division rate surpasses the DD division rate, the stem cells increase in number exponentially. Second, in contrast if the DD division rate surpasses the SS division rate, as time passes, the number of stem cells decreases and there will not be enough number of them to supply the differentiated cells and maintain the functionality of tissues.

To study the model behaviour in the face of perturbations, we examined the effect of mutations in the system. To this purpose, the fluctuations of 1000 populations, each population containing of 50 cells, are simulated by an eleven-phase simulation as it is presented in Fig 4. The mutations occur only in certain number of cells, not in every cell in an adult tissue. Therefor, in the simulations it is assumed that we only study the population of the cells (50 cells in a hypothetical adult tissue) with the chance for mutations in the genes linked to the their internal switch.

Phase 0 starts at $t = t_0$ and each population cell contains an internal two-element regulatory switch shown in Fig 1A. The model parameters are chosen from Table 1, the first row. To compute the time evolution of the cell populations, a stochastic simulation, using Gillespie algorithm, is applied. In phase 0, the state of the system in $t = t_1$, when all the cells have gone through at least two divisions, is stored. Then, phase 1 starts at $t = t_1$, the time point at which the first mutation occurs to the parameters of the cells' internal switches. In the same manner, in phase k ($k = 2, 3, \ldots, 10$) the state of the system in $t = t_{k+1}$, when all of the cells have gone

through at least $k * 2$ divisions, is stored. Then, phase $k + 1$ starts at $t = t_{k+1}$, the time point at which the kth mutation occurs to the parameters of the cells' internal switches.

All eleven phases finish at $t = T$. Similar simulations are performed for four- and six-element internal switches (shown in Fig 1B and 1C) with corresponding parameters set in Table 1, the second and third row.

In our model, mutations are represented with a random change, ϵ, in the value of the switch parameters, as following:

$$\alpha_{new} = max\{ \alpha_{old} + \epsilon , 0 \}, \tag{13}$$

where,

$$\epsilon = \begin{cases} -e & if\ 0 \leq r \leq p, \\ e & o.w., \end{cases} \tag{14}$$

with $r \sim U(0, 1)$.

Studying the mutation effects on protein structures reveals that the majority of mutations which result in amino acid substitutions, disturb the proper functionality of the proteins and lead to the malfunction of cellular processes [87–91]. Therefore, we assume that mutations in the cell internal switches rarely change the interaction to be stronger (positive-value mutations), while the majority of them either cause no significant changes in the cell functionality [92] or lead to weaken the interactions (negative-value mutations). Considering these assumptions, in our model, $e \sim Exp\left(\frac{1}{\lambda}\right)$, where λ is the mean of the Exponential distribution, and the probability of negative-value mutations, p, is chosen from the set {0.85, 0.90, 0.95, 0.99}. At time $t = t_k$ ($k = 2, 3, \ldots, 10$), in each population cell, one of the parameters $\alpha_{A_{X_1}}$, $\alpha_{I_{X_1}}$, $\alpha_{A_{Y_1}}$, and $\alpha_{I_{Y_1}}$ (α_{old}) is randomly chosen and mutated (α_{new}) based on Eq 13. It is also worth mentioning here that as the system behavior in the time interval $[t_0, t_k]$ is similar in phase 1 and k ($k = 2$, $3, \ldots, 10$), without loss of generality, one can say that all phases start from $t = t_0$.

At the end of each phase, we computed the number of populations resisting the perturbations (Fig 5), as well as the probability of generating a stem daughter cell per cell division (Fig 6). Both figures contain four subplots corresponding to the probability values of $p = 0.85$, $p = 0.90$, $p = 0.95$, and $p = 0.99$. Each subplot demonstrates three curves for two-, four-, and six-element switches. The results show that by increasing the number of mutations, the number of populations which last to the end of the simulation decreases, while the average stem cell birth rate (SCB) increases.

In our model, randomly chosen mutations values could be categorized in two groups, negative- and positive-value mutations (Eqs 13 and 14), with two completely different effects on the populations. Figs 5 and 6 reveals that negative mutation value causes the population extinction, whereas the positive one results in fast growth rate in the population. In other words, in the face of randomly chosen mutation values, two scenarios are possible for the populations.

First, in the presence of negative-value mutations occurring with high probability, the mutated stem cells are located close to the boundaries of the three-region force-field representation of Fig 2C. Therefore, in the next generation, their daughter cells are more probable to be born in the green or orange regions (as differentiated cells). In the other word, it shifts the differentiation/proliferation balance toward differentiation and increases the population extinction probability. This explains why the number of populations declines in the face of mutations (Fig 5).

In the second scenario, in some of the populations a positive-value mutation occurs with small probability. As a result, the corresponding mutated stem cell would be placed far from
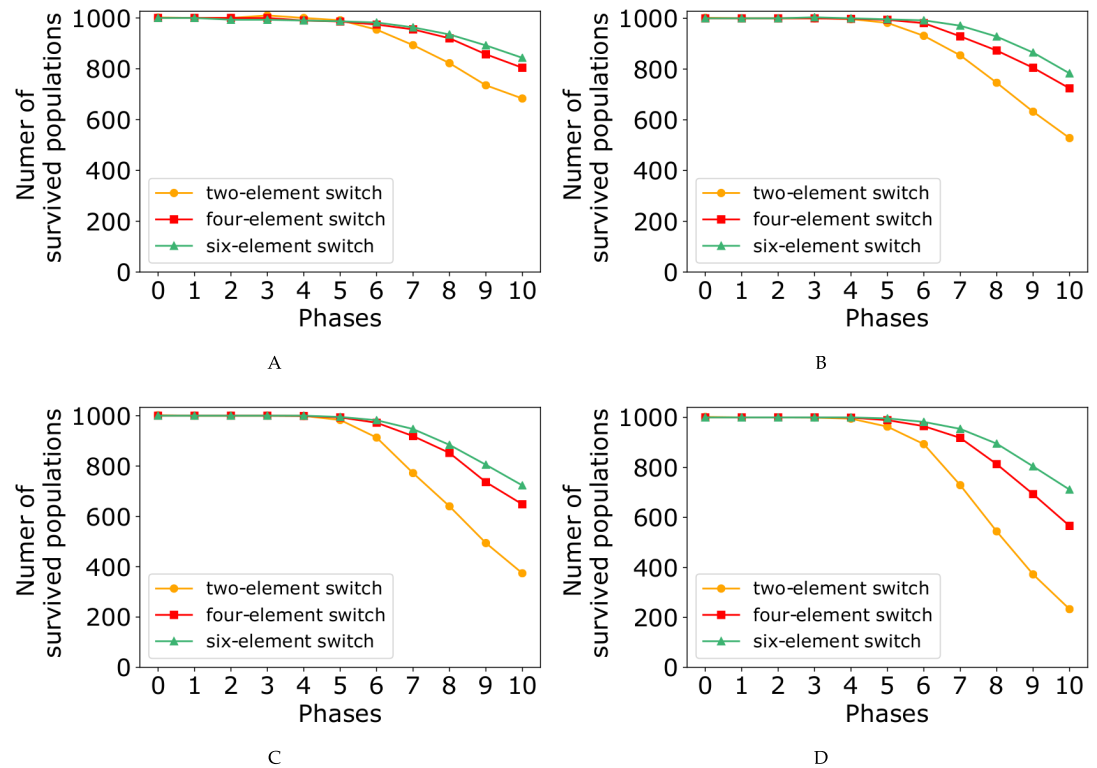
Fig 5. Number of populations survived in the face of mutations through the eleven phases of the simulation with $\lambda = 5$, and the probability value of $p = 0.85$, $p = 0.90$, $p = 0.95$, and $p = 0.99$ corresponding to subplots (A), (B), (C), and (D), respectively.

the boundaries and the original middle attractor. Therefore, in the next generation, the daughter cells are more likely to remain in the yellow region of Fig 2C (as stem cells). In contrast with the first scenario, it shifts the differentiation/proliferation balance toward proliferation and increases the population growth rate (SCB rate). This is compatible with the system behavior in the face of mutations shown in Fig 6.

In each subplot of Figs 5 and 6, it is obvious that four- and six-element switches could better buffer the perturbations effects compared to the two-element switches. It is in agreement with the great idea of Waddington, "canalisation" in [85]. Besides, the curves in Fig 5 show that the perturbation effect on the number of populations surviving to the end of simulations is more pronounced when the value of p is relatively large. In contrast, the model perturbation effect on SCB rate is weaker for the large values of p (Fig 6).

To analyze the effect of mutations on the number of populations last to the end of phase 10 (Fig 5) and on the SCB rate (Fig 6), it is necessary to study the dynamics of our model through Fig 7, S1–S11 Figs.

The force-field representations of our tristable model corresponding to each of the six simulation phases (phase 0, 2, 4, 6, 8, 10) with two-, four-, and six-element switches are demonstrated in Fig 7, S1 and S2 Figs, respectively. For these figures, it is assumed that $p = 0.85$ and $\lambda = 5$.

In each subplot, each circle represents the middle attractor of one of the cells in the population. The representative cell is the one which produces the highest proportion of stem daughter cells at the end of each phase. It is clear that the number of circles in each subplot is equal to the number of populations last to the end of each phase. To be more specific, the number of
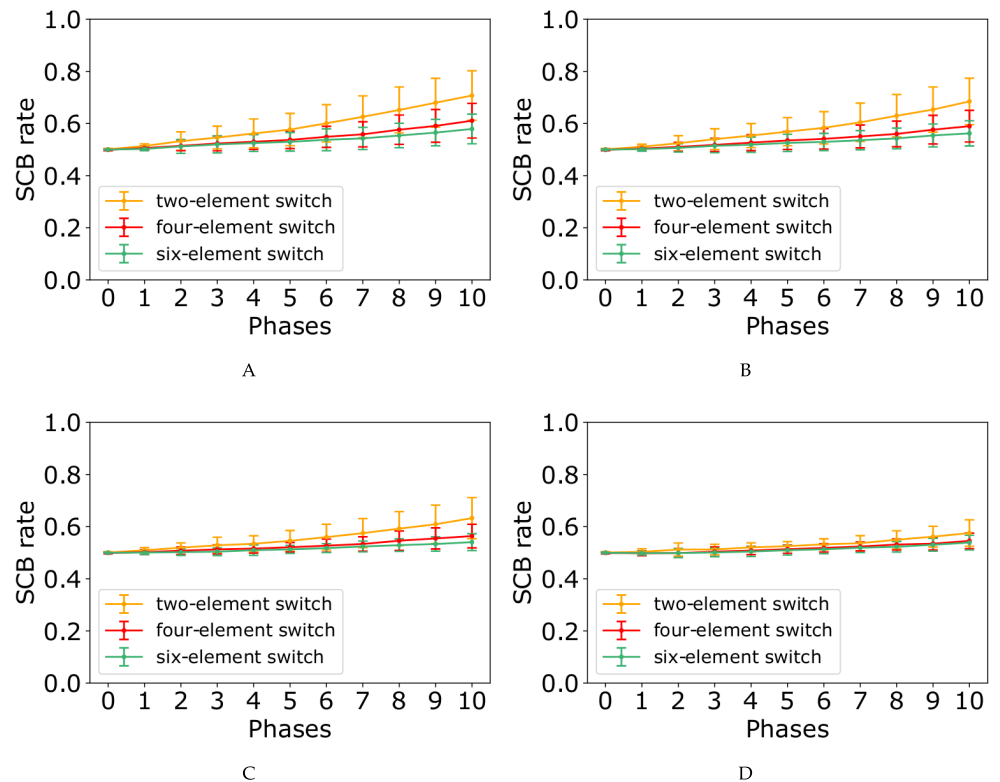
Fig 6. SCB rate in the face of mutations through the eleven phases of the simulation with λ = 5, and the probability value of $p = 0.85$, $p = 0.90$, $p = 0.95$, and $p = 0.99$ corresponding to subplots (A), (B), (C), and (D), respectively.

circles in subplots A-F in Fig 7/S1 Fig/S2 Fig correspond to the number of survived populations in phases 0, 2, 4, 6, 8, 10 in Fig 5A as yellow/red/green curve, respectively. In the same manner, S3–S11 Figs, respectively demonstrate the dynamics of our model for the probability value of $p = 0.90$, $p = 0.95$, $p = 0.99$.

Each mutation in the internal switch could easily affect the middle attractor position of the corresponding cell in the phase plane. By a single mutation with a positive (negative) value of ϵ (Eq 14), the corresponding middle attractor tends toward the upper(lower) triangular portion of force-field representation (subplot A in Fig 7, S1–S11 Figs). As mentioned previously, the growth rate of a single cell increases when its corresponding middle attractor is far from the boundaries and the original middle attractor. Since for the larger values of p ($p = 0.95$, and $p = 0.99$), positive-value mutations are less probable, most of the mutated cells attractors are located close to the boundaries and the original middle attractor (S6–S11 Figs). Therefore, most of the populations vanish in the face of mutations (Fig 5). In contrast, for the smaller values of p ($p = 0.85$, and $p = 0.90$), positive-value mutations are more probable, and most of the mutated cells attractors are located far from the boundaries and the original middle attractor in the direction of the minor diagonal of the force-field representation (Fig 7, S1–S5 Figs). Therefore, the growth rate is easily affected by mutations for the smaller values of p (Fig 6).

Studying the dynamics of our model through six subplots of each of the Fig 7, S1–S11 Figs reveal how populations facing a single mutation behave differently from the ones facing the accumulation of mutations. For the ease in discussion, since there is a one-to-one correspondence between the cells and their middle attractor, we assume that each circle represent the cell which produces the highest proportion of stem daughter cells in the population.
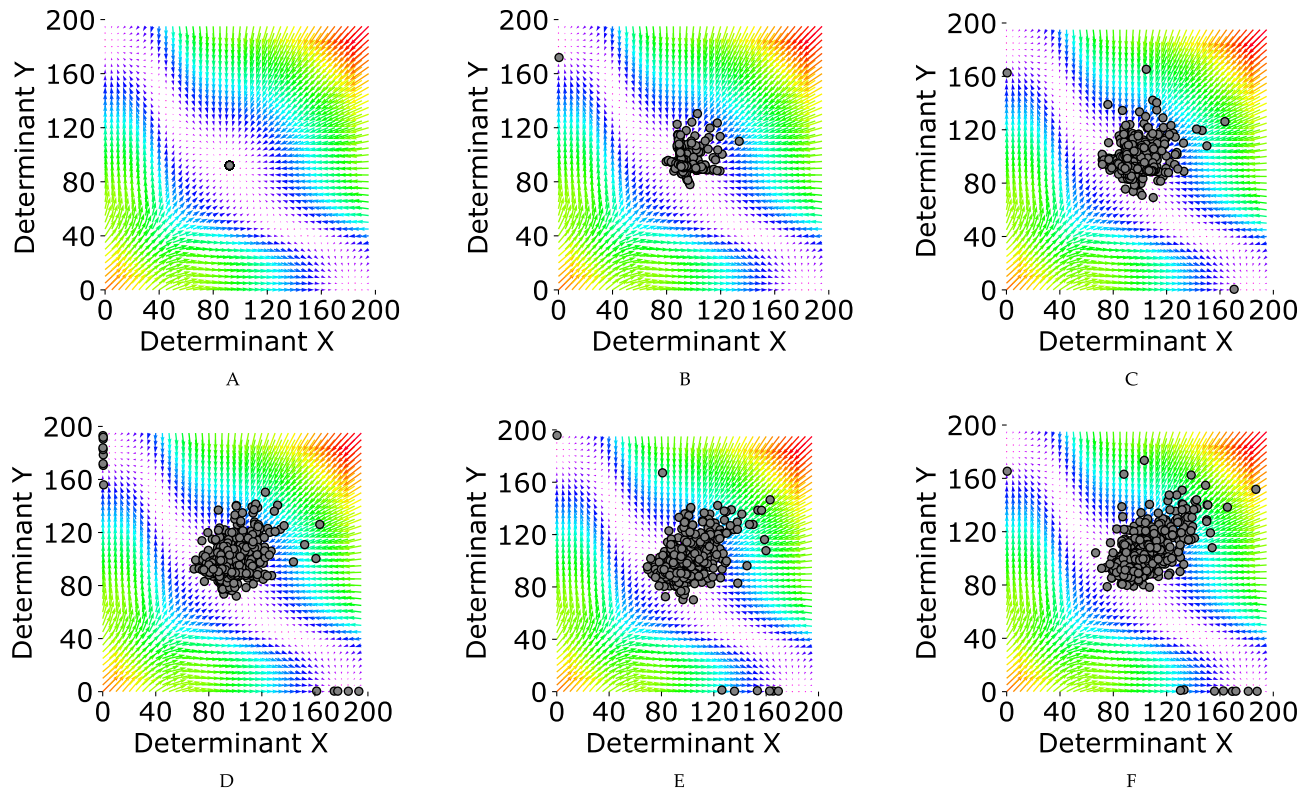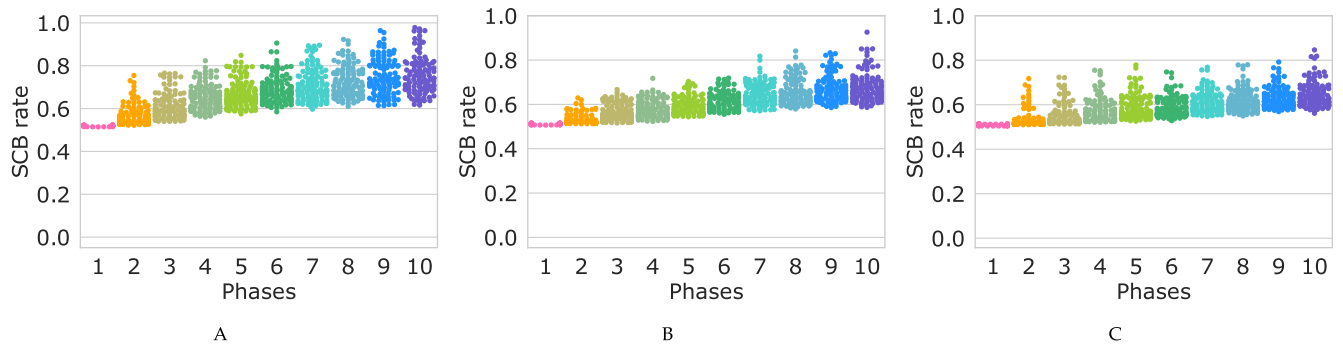
Fig 7. Six phases of the simulation with the probability value of p = 0.85, and λ = 5. The internal regulatory networks of cells are assumed to be two-element switches. (A-F) Phases 0, 2, 4, 6, 8, 10 of the simulations. In each one of the plots, each circle represents the middle attractor of one of the cells in the population, with the representative cell being the one which produces the highest proportion of stem daughter cells at the end of each phase.

When a single mutation occurs in a cell, either the cell would be located close to the boundaries and dies through the next division or it would be located far from the boundaries with a higher growth rate and remains in the population. In the same manner, in the next generation, when a single mutation occurs in a survived cell, either the cell would be located close to the boundaries and dies through the next division or it would be located far from the boundaries with a higher growth rate and remains in the population (Clearly, it is possible that for a specific cell, the growth rate is not increased by occurring the second mutation. However, in this case the cell dies in the next generation with a great chance. Therefore, without loss of generality we assume that we are studying the cells with increasing growth rate.) This process is repeated for all future mutations. One can say, if a cell remains in the population and receives the 10th mutation, it is a cell with a high growth rate (with a great chance), i.e. a cell which is far from the boundaries in the direction of the minor diagonal of the force-field representation.

Each subplot in Fig 8 (see also S12 Fig) shows the rate of stem cell birth in 50 cells with the highest growth rate, 50 cells among all the populations cells resisting the perturbations to the end of each phase. Fig 8 illustrates that accumulation of mutations could give rise to the birth of cells which always divides symmetrically to produce two daughter stem cells, cells with the SCB rate value of $\simeq$100%. In other words, mutation accumulation results in the birth of "immortal cells" which pass through several symmetric divisions which lead to exponemtially growth in population number (see S13 Fig).

Fig 8. Swarm plot of the SCB rate in ten phases of the simulation. (A, B, C) Swarm plot for the populations of cells with two-element, four-element, and six-element switches, respectively with the probability value of $p = 0.85$.

In Fig 8, and S12 Fig it is clearly seen again that more complex switches provide more robustness, and that for the larger values of p, cells with the high rate of SCB are less probable while the great number of cell populations undergo a decline contrasting with the smaller values of p.

We have designed two eleven-phase simulations corresponding to two different values, $\lambda = 2$, and $\lambda = 10$ (Eqs 13 and 14). Similar to the simulation which was described previously (Fig 4), simulations start at $t = t_0$ and stop at $t = T$, with 1000 populations with 50 cells, where each cell contains a two-element internal switch, and $p = 0.95$. Fig 9 (also see S14 Fig) shows how our model behaviour is influenced by the values of the parameter λ ($\lambda = 2$, $\lambda = 5$, and $\lambda = 10$). The dynamics of our system through ten phases of the simulations is shown in S15 and S16 Figs for $\lambda = 2$, and $\lambda = 10$, respectively. Analyzing Fig 9, S15 and S16 Figs reveals that perturbations with $\lambda = 2$ merely can affect the system behaviour, while perturbations with $\lambda = 10$ exhibit high random variation in the system behaviour.

Changing the bias of switch by changing the parameters

The proportion of cells which remain as stem cells to continue self-renewal or that which begin the the pathway to differentiation is clearly related to the area of three attractors domain (Fig 2C). In other words, the final fate of the daughter cells could be influenced by the value of
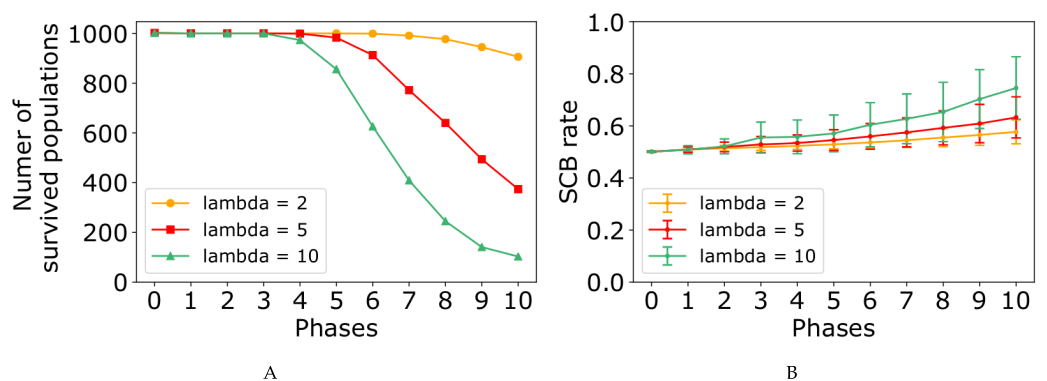
Fig 9. The system behaviour in the face of mutations through the eleven phases of the simulation with different values of parameter λ, $\lambda = 2$, $\lambda = 5$, and $\lambda = 10$. The internal regulatory networks of the cell populations are two-element switches, and the probability value of p is equal to 0.95. (A, B) SCB rate and number of populations survived in the face of mutations.
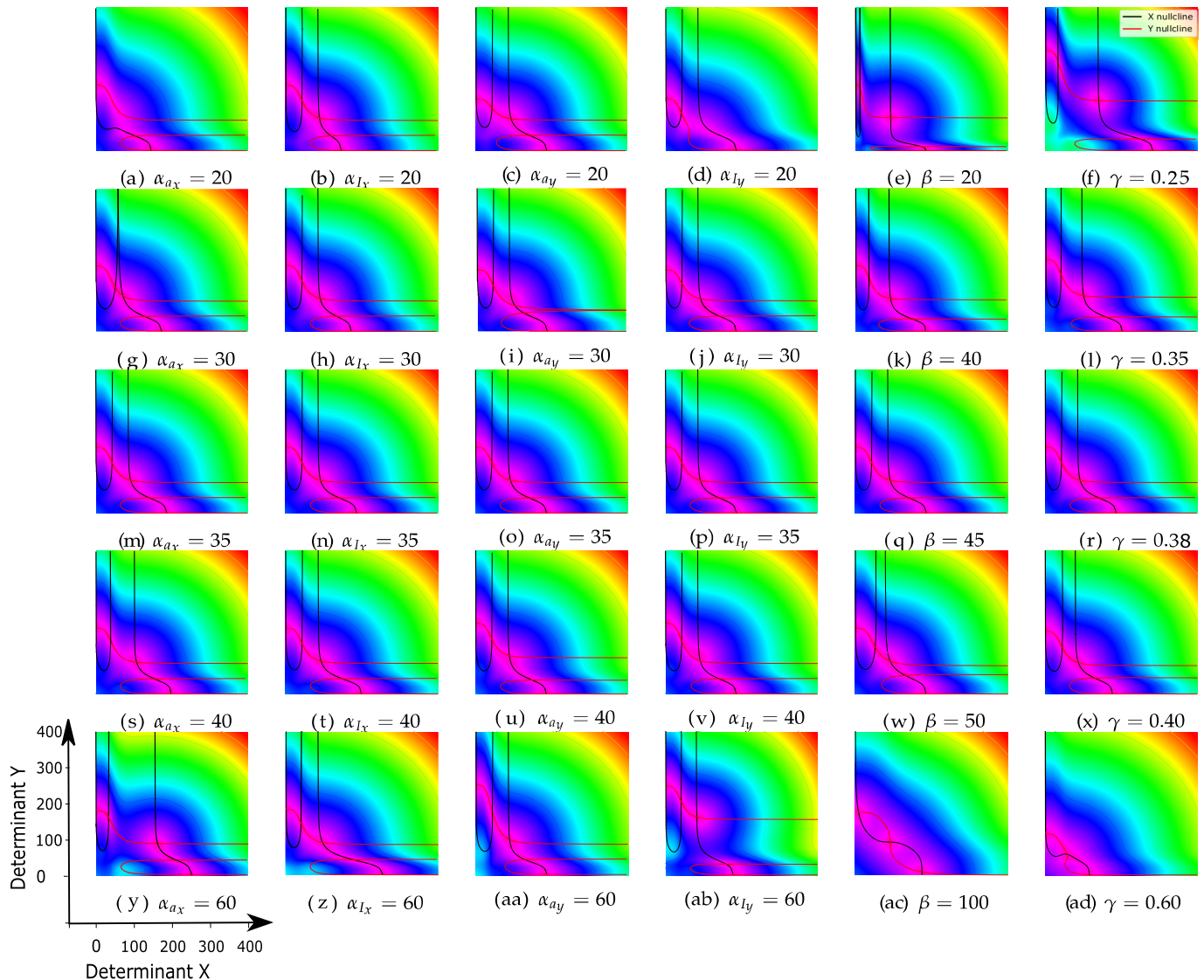
Fig 10. The system behavior in parameter space, and evaluation of the effect of parameters' changes for Eq 1. In the 5 × 6 array, each cell represents the $X - Y$ phase plane, $X-$, and $Y-$nullclines, for parameter values as indicated at the bottom of each subplot. The magenta regions represent the steady states domains. The basic set of parameters are chosen from Table 1, $\alpha_{A_{X_1}} = \alpha_{I_{X_1}} = \alpha_{A_{Y_1}} = \alpha_{I_{Y_1}} = 35$, $\beta = 45$, $\gamma = 0.38$, and $n = 4$.

the parameters in Eq 1. Besides, depending on the intensity of inhibitory and activatory effects of determinants (through the values of constants in the Hill function ([27]), the attractor domains could be symmetric or not. Fig 10 shows the system behaviour in parameter space by evaluation of the effect of six parameters ($\alpha_{A_{X_1}}$, $\alpha_{I_{X_1}}$, $\alpha_{A_{Y_1}}$, $\alpha_{I_{Y_1}}$, β, and γ) of Eq 1 in six columns.

The middle row indicates $X - Y$ phase plane, and $X-$, and $Y-$nullclines corresponding to the original set of parameters of Table 1, the first row.

Although our model describes a symmetric dynamical system, Fig 10 shows that by changing the parameters in the model it can be used to study any desired tissue with different proportion of differentiated cells. In our view, with appropriate level of stochasticity, an asymmetric switch still will be able to maintain the desired proportion of stem cells. However, in an asymmetric system the phenotypic ratio of differentiated cells (differentiated cell types A, and

B) would not be equal. In other words, regarding to the parameters set to the switch, the daughter cell birth could be either A-biased or B-biased. It reflects the flexibility of our model.

Discussion

By focusing on the effect of stochasticity on the cell final fate, we computationally modeled a regulatory mechanism to orchestrate the proliferation/differentiation balance maintaining the homeostatic state in a hypothetical adult tissue. In the most simple model, it is assumed that this hypothetical developing tissue consists of stem cells and two differentiated cell types. Our model has been described by a set of ordinary differential equations to model a regulatory switch (Eq 1). This switch consists of two cytoplasmic cell fate determinants with auto-activation and mutual inhibition (Fig 1A) which forms a tristable dynamical system. The results showed that two-element switches can be significantly affected by the system perturbations, while the more complex switches (Fig 1B and 1C) provide more robustness. This is somehow similar to the idea of "canalisation" in Waddington's book [99]. Several biological observations being collected to support the existence of internal switches consisting two groups of determinants, with feedback activation within each group and feedback inhibition between the groups [36]. Each dividing stem cell contains a small number of determinants, and a small change could significantly affect the tissue's final fate. The extended regulatory networks work as a crucial defence against the perturbations in the system. Moreover, our analysis reflects the flexibility of our model to describe any desired tissue with different proportion of differentiated cells (Fig 10).

Here, noise is defined as absolute value of the difference between the number of determinants in each cell and the expected number of them in the population, (the original middle attractor) [16, 93]. From this definition, it is immediately concluded that, the spatial arrangement of the noise would be the same as distributions of cell determinants around the attractor points on the phase plane. Therefore, one can say, the cell noise distribution balances out the proliferation and differentiation in the population to maintain homeostatic state. When the noise variation increases, the majority of the daughter cells are born as differentiated cells (in orange or green region of Fig 2C). In this case, after several generations, there wont be enough stem cells to replace the dead differentiated cells in the tissue. This can be interpreted as aging [94]. On the other hand, by decreasing the noise variation, a great number of daughter cells are born as stem cells. Under this condition, the growth rate of the cell population increases through the future generations. This can be interpreted as cancer [95]. This indicates the key role the noise plays in cell decision-making by regulating the probability of differentiation in a normal adult tissue.

Our results are in agreement with the previous study by Safdari et. al. [10] introducing a bistable system in which a cell can be divided to two daughter cells with different reversible phenotypes. Here, we also point out the prominent role of stochasticity to contribute non-genetic diversityby by extending the model by changing a bi-stable system to a tri-stable one. However, we assume that offsprings phenotypes are irreversible and do not change between states through generations. Besides, we illustrate that only the exact level of stochasticity is required to maintain homeostasis state, which is also compatible with their study.

To keep a pool of N stem cells in an adult tissue, the original stem cells must produce N stem cells. For this purpose, each division produces one stem cell and one differentiated cell, on average [3]. Without loss of generality, we can say that in homeostatic state, all the cells produce exactly one stem cell and one differentiated cell (SCB rate in phase 0 from Fig 6). When a mutation occurs in a cell, two following scenarios are possible, stem cell extinctions (Fig 5 and S13 Fig) or exponential expansion of them (Figs 6 and 8, S12 and S13 Figs).

In the former case, the mutated cell produces two differentiated cells through the next division (with a great chance). As a result, our hypothetical tissue contains $N - 1$ stem cells. Two new born daughter cells carry their mother cell's mutation. However, differentiated cells are non-dividing cells and the inherited mutation will be omitted from the population by their death. Therefore, this mutation does not affect the next generation of the cell population. In other words, the only impact of the mutation on the population is the extinction of one stem cell within the stem cell pool.

In the latter case, the mutated cell divides into two daughter stem cells (with a great chance) which leads to $N + 1$ stem cells in our hypothetical tissue. Two new born daughter cells carry their mother cell's mutation. In contrast with the former case, stem cells are dividing cells and the inherited mutation not only remains in but also spreads throughout the population via the symmetric cell divisions. Consequently, this mutation results in the exponential expansion of the stem cell pool. It resembles the behaviour of the dividing tumour cells with a strong bias toward generating dividing over non-dividing daughter cells through cell division [96].

In this study, aging is defined as a process through which the tissue gradually loses the stem cells with their self-renewal and regenerative potential. Also, cancer is defined as a process in which an individual mutant pool of stem cells divides and increase in mass, out of control. Based on these definitions and considering the consequences of single and accumulative mutations in the population, it is easily concluded that aging is a slow process while cancer can grow so fast.

Maintaining tissue homeostasis is strongly linked to the stem cell divisions with the risk of mutations in the next generation. In other words, in a long period of time and in a large enough population, mutations are inevitable [97]. When a single mutation occurs, in the genes linked to the cell internal switch, it influences the bias of the daughter cells' fate toward either cell differentiation (and death) or cell proliferation with a higher growth rate ($g_1 > 0.50$). In the former case, the mutation will be removed from the population while in the latter case the mutation remains in. In the same manner, in the next generation, when a single mutation occurs in a survived cell, either the cell dies through the next division or remains in the population with a higher growth rate ($g_2 \geq g_1 > 0.50$). This process is repeated for all future mutations. One can say, if a cell remains in the population and receives more mutation, it is a cell with a high growth rate (with a great chance). These dividing cells, with the accumulation of inherited mutations, undergo symmetric cell divisions which lead to exponential expansion of the stem cell pool in the tissue (Fig 6 and S13 Fig). It reveals how populations facing a single mutation behave differently from the ones facing the accumulation of mutations.

As it is mentioned, mutation accumulation can result in developing cancer. It clearly explains how cancer can be considered as an age-related process. In the other words, as a sufficiently long period of time is needed to grow mutated cells which multiply in great number, one can say the probability of cancer incidence increases with age [97, 98]. In addition, this is in keeping with those studies emphasizing on the importance of the total number of the stem cell divisions, to receive successive mutations, in the lifetime risk of many cancer types [97–99]. Moreover, it can be easily concluded that if someone is born with inherited genetic mutation, it puts them at a higher risk of cancer.

In tissue homeostasis, SCB rate after each stem cell division is equal to 0.50 on average. On the other words, all stem cells have similar capacity to self-renew and/or differentiate. However, analysing S13 Fig (in phase 0) reflects the fact that stem cells behave in a stochastic manner when they are studied individually. Although the size of the stem cell pool remains fixed in the tissue (Phase 0 from Fig 6), some populations shrink whereas some others expand in size [5]. S13 Fig shows that the population behaviour can be described as a gambling game with equal odds as it was discussed in [19]: *'equal chance' does not guarantee 'equal outcome'*. It

implies how the presence of controlled noise in a population of genetically similar cells with the same environmental condition provides both heterogeneity and homeostasis [6].

Although this work has been mainly focused on the noise effect on cell decision-making to maintain homeostatic state, it has not escaped our notice that intercellular signaling has a prominant role in maintaining homeostasis, and the emergence of spatiotemporal patterns [100–102]. It could be interesting to study the effect of noise in the presence of intercellular signaling on maintaining homeostasis state, and self-organization using our tri-stable switch, in a future work.

Supporting information

S1 Fig. Six phases of the simulation with the probability value of p = 0.85, and λ = 5. The internal regulatory networks of cells are assumed to be four-element switches. (A-F) Phases 0, 2, 4, 6, 8, 10 of the simulations. In each one of the plots, each circle represents the middle attractor of one of the cells in the population, with the representative cell being the one which produces the highest proportion of stem daughter cells at the end of each phase. (EPS)

S2 Fig. Six phases of the simulation with the probability value of p = 0.85, and λ = 5. The internal regulatory networks of cells are assumed to be six-element switches. (A-F) Phases 0, 2, 4, 6, 8, 10 of the simulations. In each one of the plots, each circle represents the middle attractor of one of the cells in the population, with the representative cell being the one which produces the highest proportion of stem daughter cells at the end of each phase. (EPS)

S3 Fig. Six phases of the simulation with the probability value of p = 0.90, and λ = 5. The internal regulatory networks of cells are assumed to be two-element switches. (A-F) Phases 0, 2, 4, 6, 8, 10 of the simulations. In each one of the plots, each circle represents the middle attractor of one of the cells in the population, with the representative cell being the one which produces the highest proportion of stem daughter cells at the end of each phase. (EPS)

S4 Fig. Six phases of the simulation with the probability value of p = 0.90, and λ = 5. The internal regulatory networks of cells are assumed to be four-element switches. (A-F) Phases 0, 2, 4, 6, 8, 10 of the simulations. In each one of the plots, each circle represents the middle attractor of one of the cells in the population, with the representative cell being the one which produces the highest proportion of stem daughter cells at the end of each phase. (EPS)

S5 Fig. Six phases of the simulation with the probability value of p = 0.90, and λ = 5. The internal regulatory networks of cells are assumed to be six-element switches. (A-F) Phases 0, 2, 4, 6, 8, 10 of the simulations. In each one of the plots, each circle represents the middle attractor of one of the cells in the population, with the representative cell being the one which produces the highest proportion of stem daughter cells at the end of each phase. (EPS)

S6 Fig. Six phases of the simulation with the probability value of p = 0.95, and λ = 5. The internal regulatory networks of cells are assumed to be two-element switches. (A-F) Phases 0, 2, 4, 6, 8, 10 of the simulations. In each one of the plots, each circle represents the middle attractor of one of the cells in the population, with the representative cell being the one which produces the highest proportion of stem daughter cells at the end of each phase. (EPS)

S7 Fig. Six phases of the simulation with the probability value of p = 0.95, and λ = 5. The internal regulatory networks of cells are assumed to be four-element switches. (A-F) Phases 0, 2, 4, 6, 8, 10 of the simulations. In each one of the plots, each circle represents the middle attractor of one of the cells in the population, with the representative cell being the one which produces the highest proportion of stem daughter cells at the end of each phase.
(EPS)

S8 Fig. Six phases of the simulation with the probability value of p = 0.95, and λ = 5. The internal regulatory networks of cells are assumed to be six-element switches. (A-F) Phases 0, 2, 4, 6, 8, 10 of the simulations. In each one of the plots, each circle represents the middle attractor of one of the cells in the population, with the representative cell being the one which produces the highest proportion of stem daughter cells at the end of each phase.
(EPS)

S9 Fig. Six phases of the simulation with the probability value of p = 0.99, and λ = 5. The internal regulatory networks of cells are assumed to be two-element switches. (A-F) Phases 0, 2, 4, 6, 8, 10 of the simulations. In each one of the plots, each circle represents the middle attractor of one of the cells in the population, with the representative cell being the one which produces the highest proportion of stem daughter cells at the end of each phase.
(EPS)

S10 Fig. Six phases of the simulation with the probability value of p = 0.99, and λ = 5. The internal regulatory networks of cells are assumed to be four-element switches. (A-F) Phases 0, 2, 4, 6, 8, 10 of the simulations. In each one of the plots, each circle represents the middle attractor of one of the cells in the population, with the representative cell being the one which produces the highest proportion of stem daughter cells at the end of each phase.
(EPS)

S11 Fig. Six phases of the simulation with the probability value of p = 0.99, and λ = 5. The internal regulatory networks of cells are assumed to be six-element switches. (A-F) Phases 0, 2, 4, 6, 8, 10 of the simulations. In each one of the plots, each circle represents the middle attractor of one of the cells in the population, with the representative cell being the one which produces the highest proportion of stem daughter cells at the end of each phase.
(EPS)

S12 Fig. Swarm plot of the SCB rate in ten phases of the simulation. (A, B, C) Swarm plot for the populations of cells with two-element, four-element, and six-element switches, respectively and the probability value of p = 0.90. (D, E, F) Swarm plot for the populations of cells with two-element, four-element, and six-element switches, respectively and the probability value of p = 0.95. (G, H, I) Swarm plot for the populations of cells with two-element, four-element, and six-element switches, respectively and the probability value of p = 0.99.
(EPS)

S13 Fig. Population size distribution among eleven phases of the simulation. (A, B, C) The population of cells with two-element, four-element, and six-element switches, respectively and the probability value of 0.85%. (D, E, F) The population of cells with two-element, four-element, six-element switches, respectively and the probability value of 0.90%. (G, H, I) The population of cells with two-element, four-element, six-element switches, respectively and the probability value of 0.95%. (J, K, L) The population of cells with two-element, four-element, six-element switches, respectively and the probability value of 0.99%.
(EPS)

S14 Fig. The system behaviour in the face of mutations through the eleven phases of the simulation. Simulations start with different values of parameter λ. The internal regulatory networks of the cell populations are two-element switches, and the probability value of p is equal to 0.95. (A, B, C) Phases 10 of the simulations with $\lambda = 2$, $\lambda = 5$, and $\lambda = 10$, respectively. In each one of the plots, each circle represents the middle attractor of one of the cells in the population, with the representative cell being the one which produces the highest proportion of stem daughter cells at the end of each phase (D, E, F) Swarm plot of the SCB rate with $\lambda = 2$, $\lambda = 5$, and $\lambda = 10$, respectively. (G, H, I) Population size distribution among eleven phases of the simulation with $\lambda = 2$, $\lambda = 5$, and $\lambda = 10$, respectively.
(EPS)

S15 Fig. Six phases of the simulation with the probability value of $p = 0.95$, and $\lambda = 2$. The internal regulatory networks of cells are assumed to be two-element switches. (A-F) Phases 0, 2, 4, 6, 8, 10 of the simulations. In each one of the plots, each circle represents the middle attractor of one of the cells in the population, with the representative cell being the one which produces the highest proportion of stem daughter cells at the end of each phase.
(EPS)

S16 Fig. Six phases of the simulation with the probability value of $p = 0.95$, and $\lambda = 10$. The internal regulatory networks of cells are assumed to be two-element switches. (A-F) Phases 0, 2, 4, 6, 8, 10 of the simulations. In each one of the plots, each circle represents the middle attractor of one of the cells in the population, with the representative cell being the one which produces the highest proportion of stem daughter cells at the end of each phase.
(EPS)

Acknowledgments

Author Contributions

Conceptualization: Mehdi Sadeghi.

Formal analysis: Najme Khorasani.

Methodology: Najme Khorasani.

Project administration: Mehdi Sadeghi, Abbas Nowzari-Dalini.

Supervision: Mehdi Sadeghi, Abbas Nowzari-Dalini.

Validation: Mehdi Sadeghi.

Writing – original draft: Najme Khorasani.

Writing – review & editing: Mehdi Sadeghi, Abbas Nowzari-Dalini.

References

1. Siminovitch L, McCulloch EA, Till JE. The distribution of colony-forming cells among spleen colonies. Journal of Cellular and Comparative Physiology. 1963; 62(3):327–336. PMID: 14086156

2. Simons BD, Clevers H. Strategies for homeostatic stem cell self-renewal in adult tissues. Cell. 2011; 145(6):851–862. PMID: 21663791

3. Krieger T, Simons BD. Dynamic stem cell heterogeneity. Development. 2015; 142(8):1396–1406. PMID: 25852198

4. Greulich P, Simons BD. Dynamic heterogeneity as a strategy of stem cell self-renewal. Proceedings of the National Academy of Sciences. 2016; 113(27):7509–7514.

5. Rulands S, Simons BD. Tracing cellular dynamics in tissue development, maintenance and disease. Current opinion in cell biology. 2016; 43:38–45. PMID: 27474807

6. Rulands S, Simons BD. Emergence and universality in the regulation of stem cell fate. Current Opinion in Systems Biology. 2017; 5:57–62.

7. Rulands S, Lescroart F, Chabab S, Hindley CJ, Prior N, Sznurkowska MK, et al. Universality of clone dynamics during tissue development. Nature physics. 2018; 14(5):469. https://doi.org/10.1038/s41567-018-0055-6 PMID: 29736183

8. Raser JM, O′shea EK. Noise in gene expression: origins, consequences, and control. Science. 2005; 309(5743):2010–2013. https://doi.org/10.1126/science.1105891 PMID: 16179466

9. Newman JR, Ghaemmaghami S, Ihmels J, Breslow DK, Noble M, DeRisi JL, et al. Single-cell proteomic analysis of S. cerevisiae reveals the architecture of biological noise. Nature. 2006; 441(7095):840. PMID: 16699522

10. Safdari H, Kalirad A, Picioreanu C, Tusserkani R, Goliaei B, Sadeghi M. Noise-driven Cell differentiation and the emergence spatiotemporal patterns. PLoS ONE. 2020; 15(4): e0232060. https://doi.org/10.1371/journal.pone.0232060

11. Gonze D, Gérard C, Wacquier B, Woller A, Tosenberger A, Goldbeter A, et al. Modeling-based investigation of the effect of noise in cellular systems. Frontiers in Molecular Biosciences. 2018; 5:34. https://doi.org/10.3389/fmolb.2018.00034 PMID: 29707543

12. Delbrück M. Statistical fluctuations in autocatalytic reactions. The Journal of Chemical Physics. 1940; 8(1):120–124.

13. Delbrück M. The burst size distribution in the growth of bacterial viruses (bacteriophages). Journal of bacteriology. 1945; 50(2):131.

14. Arkin A, Ross J, McAdams HH. Stochastic kinetic analysis of developmental pathway bifurcation in phage λ infected Escherichia coli cells. Genetics. 1998; 149(4):1633–1648.

15. Spudich JL, Koshland DE. Non-genetic individuality: chance in the single cell. Nature. 1976; 262 (5568):467. PMID: 958399

16. McAdams HH, Arkin A. Stochastic mechanisms in gene expression. Proceedings of the National Academy of Sciences. 1997; 94(3):814–819.

17. Losick R, Desplan C. Stochasticity and cell fate. science. 2008; 320(5872):65–68. https://doi.org/10.1126/science.1147888 PMID: 18388284

18. Clevers H. Stem cells, asymmetric division and cancer. Nature genetics. 2005; 37(10):1027. PMID: 16195718

19. Klein AM, Simons BD. Universal patterns of stem cell fate in cycling adult tissues. Development. 2011; 138(15):3103–3111. PMID: 21750026

20. Balázsi G, van Oudenaarden A, Collins JJ. Cellular decision making and biological noise: from microbes to mammals. Cell. 2011; 144(6):910–925. https://doi.org/10.1016/j.cell.2011.01.030 PMID: 21414483

21. Kirk DL. A twelve-step program for evolving multicellularity and a division of labor. BioEssays. 2005; 27(3):299–310. PMID: 15714559

22. Peter Wolk C. Heterocyst formation. Annual review of genetics. 1996; 30(1):59–78.

23. Blake WJ, Balázsi G, Kohanski MA, Isaacs FJ, Murphy KF, Kuang Y, et al. Phenotypic consequences of promoter-mediated transcriptional noise. Molecular cell. 2006; 24(6):853–865. PMID: 17189188

24. Çağatay T, Turcotte M, Elowitz MB, Garcia-Ojalvo J, Süel GM. Architecture-dependent noise discriminates functionally analogous differentiation circuits. Cell. 2009; 139(3):512–522. PMID: 19853288

25. Acar M, Mettetal JT, Van Oudenaarden A. Stochastic switching as a survival strategy in fluctuating environments. Nature genetics. 2008; 40(4):471. PMID: 18362885

26. Ptashne M. Specific binding of the λ phage repressor to λ DNA. Nature. 1967; 214(5085):232.

27. Gardner TS, Cantor CR, Collins JJ. Construction of a genetic toggle switch in Escherichia coli. Nature. 2000; 403(6767):339. PMID: 10659857

28. Shea MA, Ackers GK. The OR control system of bacteriophage lambda: A physical-chemical model for gene regulation. Journal of molecular biology. 1985; 181(2):211–230.

29. Süel GM, Garcia-Ojalvo J, Liberman LM, Elowitz MB. An excitable gene regulatory circuit induces transient cellular differentiation. Nature. 2006; 440(7083):545. PMID: 16554821

30. Süel GM, Kulkarni RP, Dworkin J, Garcia-Ojalvo J, Elowitz MB. Tunability and noise dependence in differentiation dynamics. Science. 2007; 315(5819):1716–1719. PMID: 17379809

31. Dubnau D, Lovett CM. Transformation and recombination. In: Bacillus subtilis and its Closest Relatives. American Society of Microbiology; 2002. p. 453–471.

32. Hamoen LW, Venema G, Kuipers OP. Controlling competence in Bacillus subtilis: shared use of regulators. Microbiology. 2003; 149(1):9–17. PMID: 12576575

33. Acar M, Becskei A, van Oudenaarden A. Enhancement of cellular memory by reducing stochastic transitions. Nature. 2005; 435(7039):228. PMID: 15889097

34. Chambers I, Silva J, Colby D, Nichols J, Nijmeijer B, Robertson M, et al. Nanog safeguards pluripotency and mediates germline development. Nature. 2007; 450(7173):1230. PMID: 18097409

35. Kalmar T, Lim C, Hayward P, Munoz-Descalzo S, Nichols J, Garcia-Ojalvo J, et al. Regulated fluctuations in nanog expression mediate cell fate decisions in embryonic stem cells. PLoS biology. 2009; 7 (7):e1000149. https://doi.org/10.1371/journal.pbio.1000149 PMID: 19582141

36. Sharifi-Zarchi A, Totonchi M, Khaloughi K, Karamzadeh R, Araúzo-Bravo MJ, Baharvand H, et al. Increased robustness of early embryogenesis through collective decision-making by key transcription factors. BMC systems biology. 2015; 9(1):23. https://doi.org/10.1186/s12918-015-0169-8 PMID: 26033487

37. Chen L, Wang D, Wu Z, Ma L, Daley GQ. Molecular basis of the first cell fate determination in mouse embryogenesis. Cell research. 2010; 20(9):982. PMID: 20628366

38. Bergsmedh A, Donohoe ME, Hughes RA, Hadjantonakis AK. Understanding the molecular circuitry of cell lineage specification in the early mouse embryo. Genes. 2011; 2(3):420–448. https://doi.org/10.3390/genes2030420 PMID: 24710206

39. El Samad H, Khammash M, Petzold L, Gillespie D. Stochastic modelling of gene regulatory networks. International Journal of Robust and Nonlinear Control: IFAC-Affiliated Journal. 2005; 15(15):691–711.

40. Gillespie DT. Exact stochastic simulation of coupled chemical reactions. The journal of physical chemistry. 1977; 81(25):2340–2361.

41. Ozbudak EM, Thattai M, Kurtser I, Grossman AD, Van Oudenaarden A. Regulation of noise in the expression of a single gene. Nature genetics. 2002; 31(1):69. PMID: 11967532

42. Kepler TB, Elston TC. Stochasticity in transcriptional regulation: origins, consequences, and mathematical representations. Biophysical journal. 2001; 81(6):3116–3136. https://doi.org/10.1016/S0006-3495(01)75949-8 PMID: 11720979

43. Chang HH, Hemberg M, Barahona M, Ingber DE, Huang S. Transcriptome-wide noise controls lineage choice in mammalian progenitor cells. Nature. 2008; 453(7194):544. https://doi.org/10.1038/nature06965 PMID: 18497826

44. Elowitz MB, Levine AJ, Siggia ED, Swain PS. Stochastic gene expression in a single cell. Science. 2002; 297(5584):1183–1186. PMID: 12183631

45. Maamar H, Raj A, Dubnau D. Noise in gene expression determines cell fate in Bacillus subtilis. Science. 2007; 317(5837):526–529. https://doi.org/10.1126/science.1140818 PMID: 17569828

46. Perkins TJ, Swain PS. Strategies for cellular decision-making. Molecular systems biology. 2009; 5(1). https://doi.org/10.1038/msb.2009.83 PMID: 19920811

47. Jan YN, Jan LY. Asymmetric cell division. Nature. 1998; 392(6678):775. PMID: 9572136

48. Bradshaw N, Losick R. Asymmetric division triggers cell-specific gene expression through coupled capture and stabilization of a phosphatase. Elife. 2015; 4:e08145. https://doi.org/10.7554/eLife.08145 PMID: 26465112

49. Wu J, Tzanakakis ES. Contribution of stochastic partitioning at human embryonic stem cell division to NANOG heterogeneity. PloS one. 2012; 7(11):e50715. https://doi.org/10.1371/journal.pone.0050715 PMID: 23226362

50. Pickett-Heaps JD, Gunning BE, Brown RC, Lemmon BE, Cleary AL. The cytoplast concept in dividing plant cells: cytoplasmic domains and the evolution of spatially organized cell division. American Journal of Botany. 1999; 86(2):153–172.

51. Monahan LG, Liew ATF, Bottomley AL, Harry EJ. Division site positioning in bacteria: one size does not fit all. Frontiers in microbiology. 2014; 5:19. https://doi.org/10.3389/fmicb.2014.00019 PMID: 24550892

52. Margolin W. Themes and variations in prokaryotic cell division. FEMS microbiology reviews. 2000; 24 (4):531–548. PMID: 10978550

53. Betschinger J, Knoblich JA. Dare to be different: asymmetric cell division in Drosophila, C. elegans and vertebrates. Current biology. 2004; 14(16):R674–R685. PMID: 15324689

54. Perez-Carrasco R, Guerrero P, Briscoe J, Page KM. Intrinsic noise profoundly alters the dynamics and steady state of morphogen-controlled bistable genetic switches. PLoS computational biology. 2016; 12(10):e1005154. https://doi.org/10.1371/journal.pcbi.1005154 PMID: 27768683

55. Becskei A, Séraphin B, Serrano L. Positive feedback in eukaryotic gene networks: cell differentiation by graded to binary response conversion. The EMBO journal. 2001; 20(10):2528–2535. https://doi.org/10.1093/emboj/20.10.2528 PMID: 11350942

56. Becskei A, Serrano L. Engineering stability in gene networks by autoregulation. Nature. 2000; 405 (6786):590. PMID: 10850721

57. Ozbudak EM, Thattai M, Lim HN, Shraiman BI, Van Oudenaarden A. Multistability in the lactose utilization network of Escherichia coli. Nature. 2004; 427(6976):737. PMID: 14973486

58. Simpson ML, Cox CD, Sayler GS. Frequency domain analysis of noise in autoregulated gene circuits. Proceedings of the National Academy of Sciences. 2003; 100(8):4551–4556.

59. Huang S. Reprogramming cell fates: reconciling rarity with robustness. Bioessays. 2009; 31(5):546–560. PMID: 19319911

60. Duff C, Smith-Miles K, Lopes L, Tian T. Mathematical modelling of stem cell differentiation: the PU.1–GATA-1 interaction. Journal of mathematical biology. 2012; 64(3):449–468.

61. De Mot L, Gonze D, Bessonnard S, Chazaud C, Goldbeter A, Dupont G. Cell fate specification based on tristability in the inner cell mass of mouse blastocysts. Biophysical journal. 2016; 110(3):710–722. https://doi.org/10.1016/j.bpj.2015.12.020 PMID: 26840735

62. Folguera-Blasco N, Pérez-Carrasco R, Cuyàs E, Menendez JA, Alarcón T. A multiscale model of epigenetic heterogeneity-driven cell fate decision-making. PLoS computational biology. 2019; 15(4): e1006592. https://doi.org/10.1371/journal.pcbi.1006592 PMID: 31039148

63. Enver T, Pera M, Peterson C, Andrews PW. Stem cell states, fates, and the rules of attraction. Cell stem cell. 2009; 4(5):387–397. PMID: 19427289

64. Waddington CH, et al. An introduction to modern genetics. An introduction to modern genetics. 1939.

65. Bhattacharya S, Zhang Q, Andersen ME. A deterministic map of Waddington's epigenetic landscape for cell fate specification. BMC systems biology. 2011; 5(1):85. https://doi.org/10.1186/1752-0509-5-85

66. Lu T, Volfson D, Tsimring L, Hasty J. Cellular growth and division in the Gillespie algorithm. Systems biology. 2004; 1(1):121–128. PMID: 17052122

67. Kramers HA. Brownian motion in a field of force and the diffusion model of chemical reactions. Physica. 1940; 7(4):284–304.

68. Golding I, Paulsson J, Zawilski SM, Cox EC. Real-time kinetics of gene activity in individual bacteria. Cell. 2005; 123(6):1025–1036. PMID: 16360033

69. Erban R, Chapman SJ. Stochastic modelling of reaction–diffusion processes: algorithms for bimolecular reactions. Physical biology. 2009; 6(4):046001.

70. Golding I, Paulsson J, Zawilski SM, Cox EC. Real-time kinetics of gene activity in individual bacteria. Cell. 2005; 123(6):1025–1036. PMID: 16360033

71. Guo G, Huss M, Tong GQ, Wang C, Sun LL, Clarke ND, et al. Resolution of cell fate decisions revealed by single-cell gene expression analysis from zygote to blastocyst. Developmental cell. 2010; 18 (4):675–685. PMID: 20412781

72. Chazaud C, Yamanaka Y, Pawson T, Rossant J. Early lineage segregation between epiblast and primitive endoderm in mouse blastocysts through the Grb2-MAPK pathway. Developmental cell. 2006; 10 (5):615–624. PMID: 16678776

73. Zernicka-Goetz M, Morris SA, Bruce AW. Making a firm decision: multifaceted regulation of cell fate in the early mouse embryo. Nature Reviews Genetics. 2009; 10(7):467. PMID: 19536196

74. Rossant J, Tam PP. Blastocyst lineage formation, early embryonic asymmetries and axis patterning in the mouse. Development. 2009; 136(5):701–713. PMID: 19201946

75. Andrecut M, Halley JD, Winkler DA, Huang S. A general model for binary cell fate decision gene circuits with degeneracy: indeterminacy and switch behavior in the absence of cooperativity. PloS one. 2011; 6(5):e19358. https://doi.org/10.1371/journal.pone.0019358 PMID: 21625586

76. Cockburn K, Rossant J. Making the blastocyst: lessons from the mouse. The Journal of clinical investigation. 2010; 120(4):995–1003. https://doi.org/10.1172/JCI41229 PMID: 20364097

77. Wu G, Gentile L, Fuchikami T, Sutter J, Psathaki K, Esteves TC, et al. Initiation of trophectoderm lineage specification in mouse embryos is independent of Cdx2. Development. 2010; 137(24):4159–4169. https://doi.org/10.1242/dev.056630 PMID: 21098565

78. Ema M, Mori D, Niwa H, Hasegawa Y, Yamanaka Y, Hitoshi S, et al. Krüppel-like factor 5 is essential for blastocyst development and the normal self-renewal of mouse ESCs. Cell stem cell. 2008; 3 (5):555–567.

79. Nichols J, Zevnik B, Anastassiadis K, Niwa H, Klewe-Nebenius D, Chambers I, et al. Formation of pluripotent stem cells in the mammalian embryo depends on the POU transcription factor Oct4. Cell. 1998; 95(3):379–391. PMID: 9814708

80. Plachta N, Bollenbach T, Pease S, Fraser SE, Pantazis P. Oct4 kinetics predict cell lineage patterning in the early mammalian embryo. Nature cell biology. 2011; 13(2):117. PMID: 21258368

81. Jaenisch R, Young R. Stem cells, the molecular circuitry of pluripotency and nuclear reprogramming. Cell. 2008; 132(4):567–582. https://doi.org/10.1016/j.cell.2008.01.015 PMID: 18295576

82. Young RA. Control of the embryonic stem cell state. Cell. 2011; 144(6):940–954. https://doi.org/10.1016/j.cell.2011.01.032 PMID: 21414485

83. Avilion AA, Nicolis SK, Pevny LH, Perez L, Vivian N, Lovell-Badge R. Multipotent cell lineages in early mouse development depend on SOX2 function. Genes & development. 2003; 17(1):126–140.

84. Chambers I, Tomlinson SR. The transcriptional foundation of pluripotency. Development. 2009; 136 (14):2311–2322. https://doi.org/10.1242/dev.024398 PMID: 19542351

85. Waddington CH. The strategy of the genes. Routledge; 2014.

86. Alberts B, Johnson A, Lewis J, Raff M, Roberts K, Walter P. Epidermis and Its Renewal by Stem Cells. In: Molecular Biology of the Cell. 4th edition. Garland Science; 2002.

87. Doss CGP, Rajith B, Garwasis N, Mathew PR, Raju AS, Apoorva K, et al. Screening of mutations affecting protein stability and dynamics of FGFR1—A simulation analysis. Applied & translational genomics. 2012; 1:37–43.

88. Ng PC, Henikoff S. SIFT: Predicting amino acid changes that affect protein function. Nucleic acids research. 2003; 31(13):3812–3814. https://doi.org/10.1093/nar/gkg509 PMID: 12824425

89. Adzhubei IA, Schmidt S, Peshkin L, Ramensky VE, Gerasimova A, Bork P, et al. A method and server for predicting damaging missense mutations. Nature methods. 2010; 7(4):248–249. https://doi.org/10.1038/nmeth0410-248 PMID: 20354512

90. Capriotti E, Fariselli P, Rossi I, Casadio R. A three-state prediction of single point mutations on protein stability changes. BMC bioinformatics. 2008; 9(2):S6. https://doi.org/10.1186/1471-2105-9-S2-S6 PMID: 18387208

91. Bromberg Y, Yachdav G, Rost B. SNAP predicts effect of mutations on protein function. Bioinformatics. 2008; 24(20):2397–2398. https://doi.org/10.1093/bioinformatics/btn435 PMID: 18757876

92. Alberts B, Johnson A, Lewis J, Morgan D, Raff M, Roberts K, et al. Molecular biology of the cell, 6th edition. Garland Science; 2015.

93. Tsimring LS. Noise in biology. Reports on Progress in Physics. 2014; 77(2):026601. https://doi.org/10.1088/0034-4885/77/2/026601 PMID: 24444693

94. Schultz MB, Sinclair DA. When stem cells grow old: phenotypes and mechanisms of stem cell aging. Development. 2016; 143(1):3–14. https://doi.org/10.1242/dev.130633 PMID: 26732838

95. Sonnenschein C, Soto AM, Rangarajan A, Kulkarni P. Competing views on cancer. Journal of biosciences. 2014; 39(2):281–302. https://doi.org/10.1007/s12038-013-9403-y PMID: 24736160

96. Frede J, Greulich P, Nagy T, Simons BD, Jones PH. A single dividing cell population with imbalanced fate drives oesophageal tumour growth. Nature cell biology. 2016; 18(9):967. https://doi.org/10.1038/ncb3400 PMID: 27548914

97. Nordling C. A new theory on the cancer-inducing mechanism. British journal of cancer. 1953; 7(1):68. https://doi.org/10.1038/bjc.1953.8

98. Armitage P, Doll R. The age distribution of cancer and a multi-stage theory of carcinogenesis. British journal of cancer. 1954; 8(1):1. https://doi.org/10.1038/bjc.1954.1 PMID: 13172380

99. Tomasetti C, Vogelstein B. Variation in cancer risk among tissues can be explained by the number of stem cell divisions. Science (New York, NY). 2015; 347(6217):78.

100. Ceafalan LC, Enciu AM, Fertig TE, Popescu BO, Gherghiceanu M, Hinescu ME, et al. Heterocellular molecular contacts in the mammalian stem cell niche. European journal of cell biology. 2018; 97 (6):442–461. PMID: 30025618

101. Warmflash A, Sorre B, Etoc F, Siggia ED, Brivanlou AH. A method to recapitulate early embryonic spatial patterning in human embryonic stem cells. Nature methods. 2014; 11(8):847. https://doi.org/10.1038/nmeth.3016 PMID: 24973948

102. Guisoni N, Martinez-Corral R, Garcia-Ojalvo J, de Navascués J. Diversity of fate outcomes in cell pairs under lateral inhibition. Development. 2017; 144(7):1177–1186. PMID: 28174242